LANGMUIR

pubs.acs.org/Langmuir Article

# Bubble Rupture and Bursting Velocity of Complex Fluids

Nicola Antonio Di Spirito, Shadi Mirzaagha, Ernesto Di Maio, Nino Grizzuti, and Rossana Pasquino*

Cite This: https://doi.org/10.1021/acs.langmuir.2c01875 Read Online

ACCESS | Metrics & More | Article Recommendations | Supporting Information

**ABSTRACT:** We analyzed bubble rupture and hole opening dynamics in a non-Newtonian fluid by investigating the retraction process of thin films after inflation at different blowing rates. The experiments were modeled through a dimensional analysis, with the aim of establishing a general approach on the bubble rupture dynamics and discerning the role of viscous, elastic, surface, and inertial forces on the opening velocity, according to the nature of the specific fluid. A new mathematical model, which includes all possible contributions to the hole opening dynamics, was proposed, to the best of our knowledge for the first time. The experimental evidence on the opening velocity as a function of the inflation rate was found to be in good agreement with the prediction of the model. The sensitivity of our modeling was tested by comparing our results with the existing models of retracting velocity.

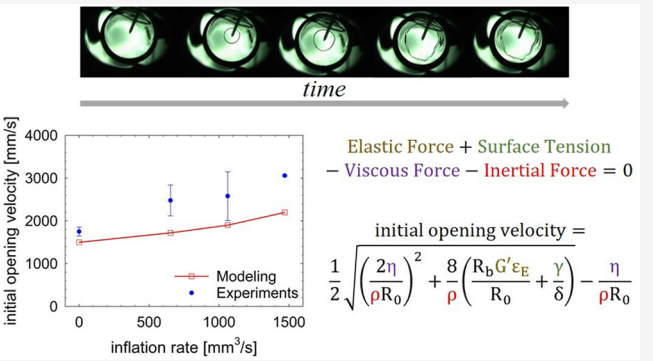


## INTRODUCTION

Bubble rupture and liquid sheet retraction are of paramount importance in many scientific and technological fields and areas of daily life,[1] such as aerosol formation,[2−5] bubbly magma rheology,[6−9] industrial and food foam processes,[10] and biology and drug delivery.

The first studies on the rupture of bubbles were performed in the second half of 1800 by Dupré[11] and Rayleigh,[12] who observed soap bubbles during their bursting. Later, Ranz[13] presented an experimental work about soap films and their bursting after a puncture, describing the role of surface tension during film retraction and found that the retracting velocity was nearly constant. A decade later, Taylor[14] and Culick[15] tried to apply a theoretical approach to Dupré derivations.[11] Specifically, they inferred a mathematical relation for the film retracting velocity $U$

$$U = \frac{dr}{dt} = \sqrt{\frac{2\gamma}{\rho\delta}} \tag{1}$$

where $dr/dt$ is the variation of the hole radius with respect to time, $\gamma$ the surface tension between the liquid and the surrounding gas, $\rho$ the density of the liquid, and $\delta$ the thickness of the film. Taylor and Culick's study was subsequently corroborated by McEntee and Mysels,[16] who experimentally studied the bursting of soap films. Keller,[17] years later, theoretically analyzed the rupture of nonuniform liquid sheets. The previous studies involved inviscid liquid films, such as water sheets or soap films in air. The first study on viscous fluids was performed by Debrégeas et al.,[18,19] who investigated the effects of viscous contribution when inertia can be considered negligible. They found that, because of the high viscosity of the fluid, the film retracting velocity is slower than in the inviscid case, and is not a constant, in contrast with the prediction of eq 1. Debrégeas et al.[18,19] proposed the following time-evolving growth law for the hole radius, $r(t)$:

$$r(t) = R_0 \exp\left(\frac{\gamma t}{\eta\delta}\right) \tag{2}$$

where $R_0$ and $\eta$ are the initial hole radius and the fluid viscosity, respectively. The initial retracting velocity of the film, $v_0^V$, is therefore

$$v_0^V = \frac{R_0\gamma}{\eta\delta} \tag{3}$$

Evers et al.[20] studied the retraction process of very thin viscoelastic films initially at rest, observing a retraction velocity much slower than that of Newtonian films because of the intrinsic film elasticity. Brenner and Gueyffier[21] focused on retraction phenomena and rim formation of very viscous films, demonstrating the importance of viscous, surface tension, and inertial contributions. Brenner and Gueyffier's analysis was enriched with numerical investigations by Song and Tryggvason,[22] who considered the effect of an ambient fluid around the film, and then by Sünderhauf et al.,[23] who focused

Received: July 17, 2022
Revised: October 7, 2022

on the presence of inertia or viscosity. Dalnoki-Veress et al.[24] investigated the formation and growth of holes in polymer films. Bubble rupture at a free surface was numerically studied by Duchemin et al.,[25] who used direct numerical simulations based on the Navier−Stokes equations. In 2009, Savva and Bush[26] presented an analysis on the retraction of planar and circular liquid sheets, highlighting the role of the viscosity contribution, geometry, and initial conditions. Later, Villone et al.[27,28] used numerical simulations to investigate the retracting process of viscoelastic films. Sabadini et al.[29] experimentally investigated the effects of the elastic contribution in soap bubbles. Then, Tammaro et al.[30] gave a complete explanation of the role of elasticity, showing that, besides the properties of the fluid and the geometry of the bubble, the inflation process and the deformation history must be considered. They found a mathematical expression of the initial retracting velocity, $v_0^E$, for a viscoelastic bubble, which accounts for both viscous forces and elasticity and neglects inertia:

$$v_0^E = \frac{R_0\gamma}{\eta\delta} + \frac{R_b G'\varepsilon_E}{\eta} \tag{4}$$

where $R_b$ represents the initial radius of the bubble, $G'$ is the fluid elastic modulus, and $\varepsilon_E$ is the recoverable deformation. Equation 4 was obtained from a force balance that includes surface tension and elastic contributions, which promote hole bursting, and the viscous contribution, which, on the other hand, slows down the opening process. It shows the dependence of the initial retracting velocity of a viscoelastic fluid on the inflation rate and on the initial bubble radius. Walls et al.[31] analyzed the role of gravity and the viscous contribution in jet drops. Furthermore, bubble rupture and droplet ejection were experimentally investigated by Ghabache and Séon,[32] who examined the size of the top jet drop after the bursting of a bubble. The formation of a liquid jet in bubble bursting, with consequent formation of emitted droplets, was studied by Ganan-Calvo,[33] who proposed a scaling law of the droplet size and jet velocity. Lai et al.[34] published a study on the dynamics of bubble rupture, describing the collapse of the cavity and the production of a jet, considering the influence of capillary inertia and viscous forces. The minimum size of the drops ejected from the rupture of a bubble was investigated by Brasz et al.,[35] who adopted high-speed camera visualization and numerical calculation. Deike et al.[36] focused on the jet velocity by means of experiments and simulations. Botta et al.[37] conducted experimental studies on soap bubble rupture, recording the phenomena of bursting by means of a high-speed camera and experimentally identifying the parameters of the materials. Then, Sen et al.[38] investigated the effects of viscoelasticity in inkjet printing to avoid satellite droplet formation. Gañán−Calvo and López−Herrera[39] analyzed bubble bursting, proposing the prediction of the size and speed of ejected droplets. Tammaro et al.[40] analyzed the role of surface viscoelasticity in bubble rupture, illustrating the circumstances under which bubbles exhibit a flowering-like morphology during bursting. Sanjay et al.[41] numerically studied the formation of capillary waves of bursting bubbles in a viscoplastic medium. Very recently, the impact of material properties, such as surface tension, viscosity, and density, on the production of gas jets from bubble bursting was examined by Dasouqi et al.[42]

Understanding the bubble rupture phenomena and the corresponding complex fluid dynamics proves to be nontrivial because of the presence of different forces acting on the system. It is not a case, indeed, that eqs 1, 3, and 4 refer to the same quantity, which is the retracting velocity, although named with different symbologies to mark specific predominances. A good approach to tackle such problems to a significant extent is the use of dimensional analysis,[43] in a way to fully understand the forces at play and their relative magnitude. The introduction of specific dimensionless groups is particularly useful in understanding the behavior of complex fluids. To this end, three important dimensionless parameters may be considered:[44] Reynolds number, $Re = \rho v\delta/\eta$, capillary number, $Ca = \eta v/\gamma$, and Weissenberg number, $Wi = \lambda v/\delta$, where v represents a characteristic velocity, $\delta$ is a characteristic length, and $\lambda$ stands for the relaxation time of the fluid. $Re$ allows for a comparison between inertial and viscous forces. $Ca$ represents the relative effect of viscous to surface forces. $Wi$ compares elastic and viscous forces. The ratio $Wi/Re$ defines the elasticity number,[45] $El = \eta\lambda/\rho\delta^2$ − that is, the comparison between inertial contributions and elasticity. The relation $Re/Ca$ results in the inverse of the squared Ohnesorge number, $Oh^{-2} = \rho\gamma\delta/\eta^2$.[46] Elastic and capillary effects vs viscous contributions can be described by the elasto-capillary number,[47] $E_c = Wi/Ca = \lambda\gamma/\eta\delta$. Depending on the fluid properties and flow conditions, the phenomenon can be described based on the magnitude of these significant dimensionless parameters.

In this paper, bubble rupture and retraction phenomena were investigated experimentally on a non-Newtonian, viscoelastic fluid, suitably chosen for its rheological properties. Furthermore, the balance of different forces governing the system was studied, and a generalized approach based on dimensional analysis was proposed. Specifically, we used a Carbopol solution as the test material since it represents an ideal candidate to test the effectiveness of dimensional analysis when all forces at play must be contemplated. Film retracting velocities following bubble rupture were experimentally determined and compared with those evaluated by using a novel theoretical equation derived from dimensional analysis. To assess the sensitivity of our mathematical model, we compared it with existing models of retracting velocity.

## MATERIALS AND METHODS

**Materials.** A water-based solution of an acrylic acid-based polymer — Carbopol Ultrez 10 (Lubrizol Co., Wickliffe, OH) — was used to perform bubble rupture experiments. The polymer was dispersed in demineralized water at room temperature and mechanically stirred to guarantee a homogeneous distribution.[48] The rheology of the solution is strongly dependent on polymer concentration and pH.[49,50] In this case, a 0.10 wt % Carbopol solution at pH 8.30 was used.

**Rheological Characterization.** The rheological properties of the fluid were experimentally studied by a stress-controlled rheometer (MCR702; Anton Paar GmbH, Graz, Austria), equipped with cone-plate geometries (CP 50-1: diameter 50 mm and cone angle 1° and CP 25-1: diameter 25 mm and cone angle 1°). Flow curve tests were performed in a range of shear rates between 100 and $10^{-5}$ $s^{-1}$, at 25 °C. Moreover, the sample viscoelasticity was studied by frequency sweep tests at 25 °C — in an angular frequency range between 100 and 0.10 rad/s — both at strains low enough to guarantee the linear viscoelastic regime and at a stress value able to simulate the rheological behavior of the fluid, once punctured.

**Bubble Rupture Analysis.** The investigation of the bubble rupture process was conducted considering a homemade apparatus and blowing protocol as used by Tammaro et al.[30] to visualize the bubble rupture and measure the retracting velocity of the hole opening. Thin flat films of fluids were deposited on a metallic cylinder with a radius of 9 mm. The film was inflated by air injected from a


https://doi.org/10.1021/acs.langmuir.2c01875
Langmuir XXXX, XXX, XXX−XXX

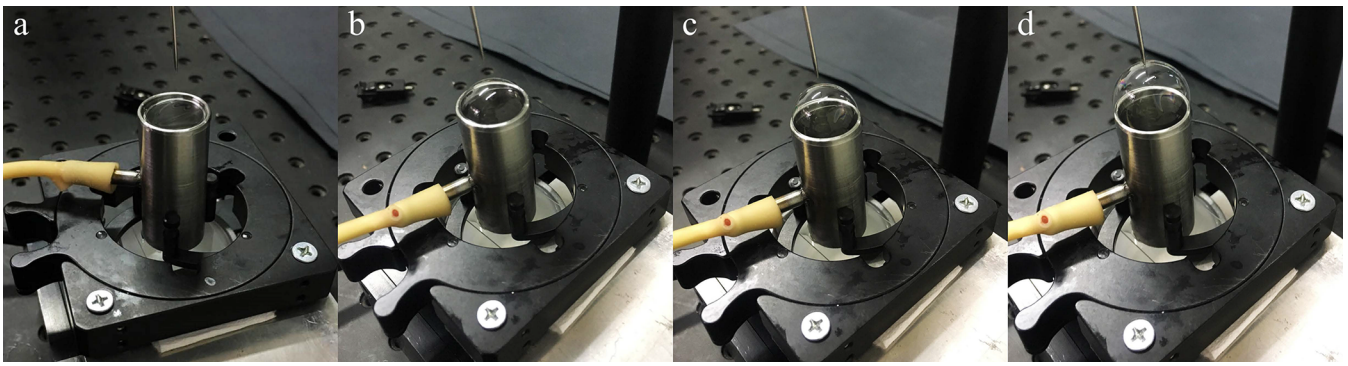


**Figure 1.** Blowing process steps: (a) film formation; (b) start of bubble inflation; (c) growth of the bubble; (d) bubble collision against the needle.

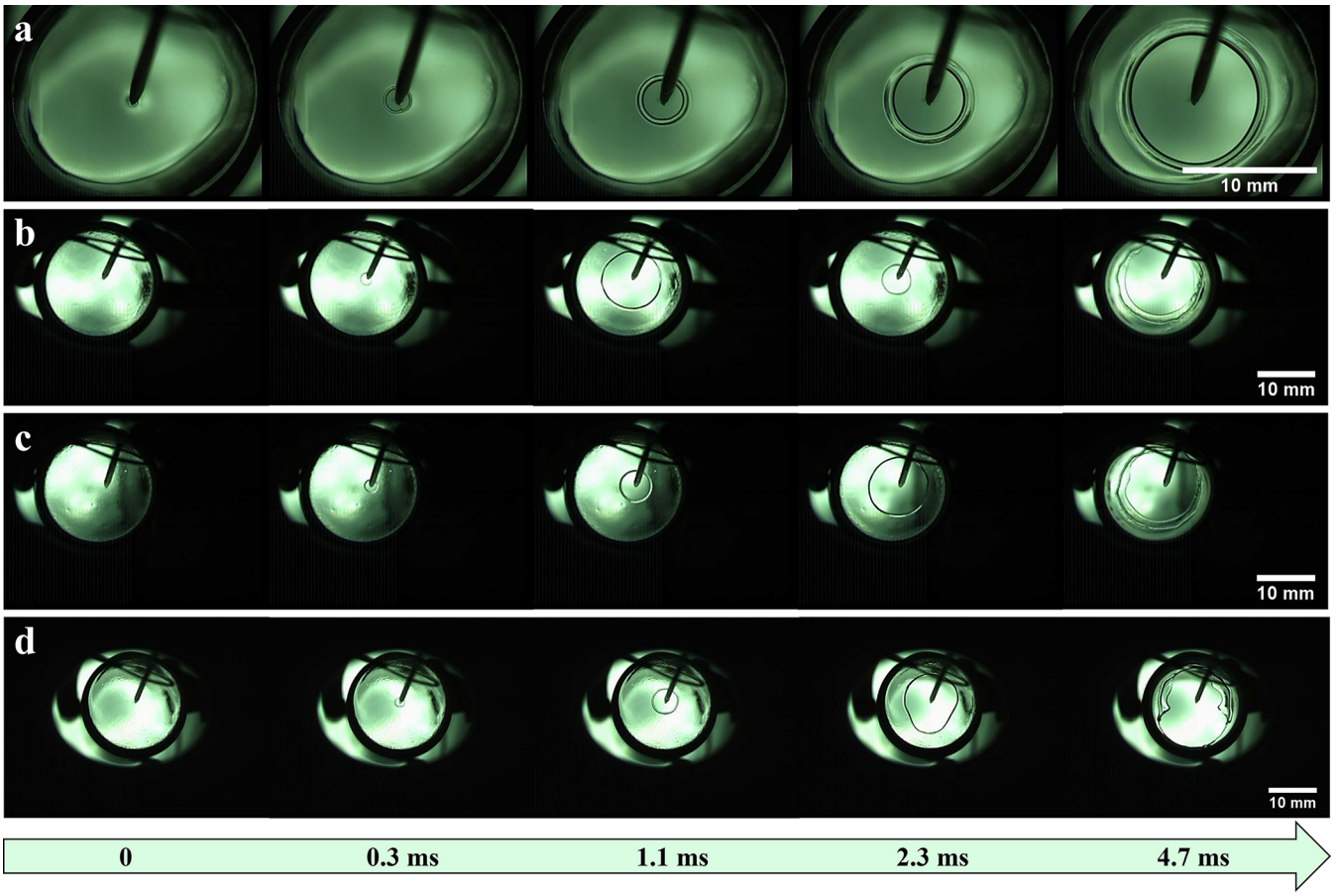


**Figure 2.** Experimental images of the bubble opening sequence for the 0.10 wt % Carbopol solution at different $Q$ values: (a) $Q = 0$; (b) $Q = 653$ mm$^3$/s; (c) $Q = 1062$ mm$^3$/s; (d) $Q = 1470$ mm$^3$/s. The timestamps of the snapshots are shown in the green arrow.

syringe pump (Model 22 syringe pump; Harvard Apparatus, Holliston, MA) through a silicone tube, at different flow rates $Q$. A needle with a tip with a radius of 62 $\mu$m was placed on top of the blown film, to puncture and break the bubble. A high-speed camera capable of acquiring up to $10^5$ frames/s (i-speed 3; Olympus Scientific Solutions, Waltham, MA) was used during bubble bursting analysis to record the bubble rupture and the subsequent film retraction stage (with a frame rate of $1.5 \times 10^4$ frames/s). Optimal light conditions, required for high-speed recording, were guaranteed by a 75 W LED lamp placed behind the film, chosen so that the light source did not significantly heat the film by radiation. In Figure 1a–d, the blowing process steps, from film formation to bubble collision against the needle, are shown.

The acquired digital frames were analyzed using ImageJ free software to measure the hole radius during film retraction as a function of time, $r(t)$. From these data, the initial hole opening retracting velocity, $v_0$, was computed considering the very early times of the radius vs time plot. As an example, Figure 2a–d shows the acquired images of the opening films of the 0.10 wt % Carbopol solution during the inflation process at different inflation rates.

Figure 2 reveals the presence of a jagged profile of the rim, which is more apparent when the inflation rate is increased. These fractured shapes are probably explained by a high $E_c$ and a high deformation rate. Under such conditions, cracks on the opening liquid film appear in the final stages, as already reported by Tammaro et al.[40] However, this morphological profile does not affect the hole opening and the film retracting velocity during the initial bubble bursting times.

A standard secondary webcam (HD Pro C920; Logitech Europe S.A., Lausanne, Switzerland) was used for macroscopic observation of the process, to measure the recoverable deformation, $\varepsilon_E$, imposed by


https://doi.org/10.1021/acs.langmuir.2c01875
Langmuir XXXX, XXX, XXX−XXX

the blowing apparatus on the liquid film. In particular, bubble growth during inflation was measured, and the variation of the bubble arc over time was calculated using ImageJ software. $\varepsilon_E$ was estimated from the total applied deformation, $\varepsilon_T$, as $\varepsilon_E \approx \varepsilon_T \exp(-\tau_i/\lambda)$,[30] where $\tau_i$ and $\lambda$ are the inflation time and the fluid relaxation time, respectively. $\varepsilon_T$ can be experimentally measured as $(a_f - a_i)/a_i$,[30] where $a_f$ represents the arc measured at $\tau_i$ and $a_i$ corresponds to the diameter of the flat film before the start of the blowing process (Figure 3).

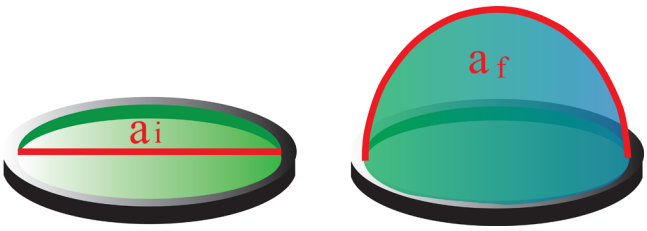


**Figure 3.** Sketch of the time evolution of the bubble arc.

The method adopted to compute the thickness of the liquid films, $\delta$, was based on measuring the weight of the amount of liquid at bubble rupture. After the deposition of the fluid on the metallic cylinder and the inflation procedure, the bubble was formed, and its breakage was performed against a sheet of paper. The fluid ring was weighed, and its thickness was computed as $\delta = m/(\rho A)$, where $m$ and $A$ are its mass and its "printed" area, respectively. $\delta$ was assumed to be uniform.

All experiments were conducted at room temperature.

## RESULTS AND DISCUSSION

**Rheology.** The flow curve of the Carbopol sample, relating the shear stress ($\sigma$) to the shear rate ($\dot{\gamma}$), is represented in Figure 4. The viscosity of the fluid decreases with increasing

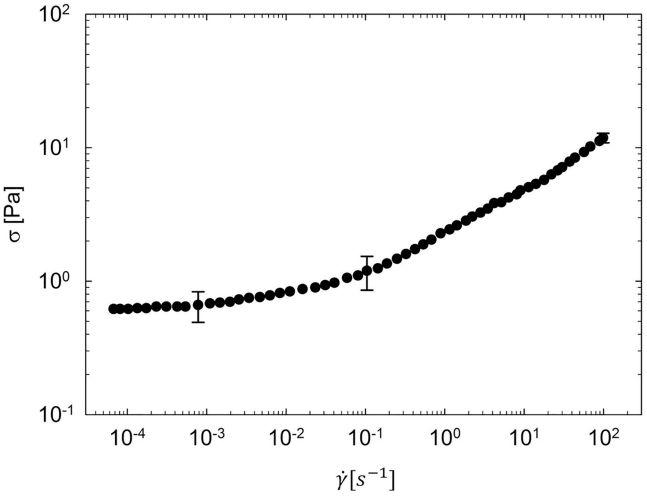


**Figure 4.** Flow curve of the Carbopol sample at 25 °C. The error bars are evaluated as the standard deviation of multiple experiments.

shear rate, showing a shear thinning behavior when a characteristic yield stress value is overcome. The curve was fitted using the Herschel–Bulkley model (eq 5)

$$\begin{cases} \sigma = \sigma_y + k\dot{\gamma}^n & \text{for } \sigma > \sigma_y \\ \dot{\gamma} = 0 & \text{for } \sigma < \sigma_y \end{cases} \quad (5)$$

where $k$ and $n$ are the consistency and flow indices, respectively, and $\sigma_y$ is the yield stress. Specifically, $k$, $n$, and $\sigma_y$ are equal to $1.6 \pm 0.1$ Pa·s$^n$, $0.42 \pm 0.01$, and $0.58 \pm 0.05$ Pa, respectively. The rheological behavior of the Carbopol solution was further characterized by frequency sweep tests. Figure 5a depicts the viscoelastic moduli of the sample, $G'$ and $G''$, at 25 °C and low strain, before yielding. The system shows solid-like behavior in the whole frequency range, as suggested by the storage modulus $G'$ being larger than the loss modulus $G''$. Linear viscoelasticity consolidates the existence of a yield stress, as shown by the $G'$ plateau at low frequencies.[51]

A frequency sweep test was also performed by imposing a stress value equal to 1 Pa. This value of stress is an estimation of the stress felt by the fluid during the blowing process, evaluated by taking into consideration the measured deformation rate (i.e., the total deformation over the inflation time) and the fluid constitutive equation (i.e., by approximating the measured deformation rate with the shear rate). More specifically, Figure 5b reports $G'$ and $G''$ on the yielded sample at a stress of 1 Pa, higher than the yield stress value. The rheological response reported in Figure 5b is distinctive of a viscoelastic polymer network, with a well-defined crossover angular frequency (i.e., a long relaxation time) and a marked elasticity.[52] These are the rheological characteristics of the sample that is punched by the needle after the blowing process.

**Bubble Rupture.** The transient hole radius, $r(t)$, after bubble rupture was investigated experimentally. During the bubble formation process, different values of the inflation rate, $Q$, were considered. Figure 6 shows $r(t)$ under static conditions (no inflation, $Q = 0$) and at different inflation rates for the Carbopol/water mixture.

In particular, $v_0$ was evaluated by a linear regression of the hole radius at the early times. As an example, Figure 7 illustrates the fit at $Q = 1470$ mm$^3$/s for our tested solution.

Table 1 lists the mean values of the resulting initial retracting velocities, $v_0$, which were computed at the beginning of the phenomenon, at different inflation rates, along with the estimated uncertainty.

**Modeling.** Bubble rupture dynamics is governed by the presence of various forces acting on the system that, therefore, must be considered when computing the bursting velocity. In general, assuming the gravity force as negligible, the retracting velocity of the film after the bubble rupture depends on different acting contributions: the elastic force, $F_E = 4\pi\delta R_b G' \varepsilon_E$, the viscous force, $F_V = -4\pi\delta v_0 \eta$, the inertial force, $F_I = -2\pi\delta R_0 \rho v_0^2$, and the surface tension, $F_\gamma = 4\pi R_0 \gamma$. While $F_E$ and $F_\gamma$ promote film retraction (both with a positive sign), $F_V$ and $F_I$ slow down hole opening (both with a negative sign). A force balance can be written as follows:

$$F_E + F_V + F_I + F_\gamma = 0 \quad (6)$$

Table 2 represents an identity card of our investigated fluid, giving a summary of the material properties that were considered to compute the dimensionless parameters discussed previously, at different inflation rates. In addition, it reports the recoverable deformation $\varepsilon_E$, measured at different $Q$ values (obviously, without inflation, $\varepsilon_E = 0$). To estimate $\varepsilon_E$, when $Q \neq 0$, the fluid relaxation time has been evaluated as the inverse of the angular frequency at which the crossover between $G'$ and $G''$ appears (see Figure 5b), i.e., $\lambda \cong 2.5$ s. Furthermore, the inflation time, $\tau_i$, decreases with increasing inflation rate ($\tau_i \cong 3$ s, at $Q = 653$ mm$^3$/s; $\tau_i \cong 2$ s, at $Q = 1062$ mm$^3$/s; $\tau_i \cong 1$ s, at $Q = 1470$ mm$^3$/s). The corresponding values of $Re$, $Ca$, $Wi$, $Oh^{-2}$, $El$, and $E_c$ are shown in Table 3. For $Q = 0$, the sample is considered unyielded with a relaxation time ideally infinite.


https://doi.org/10.1021/acs.langmuir.2c01875
Langmuir XXXX, XXX, XXX−XXX

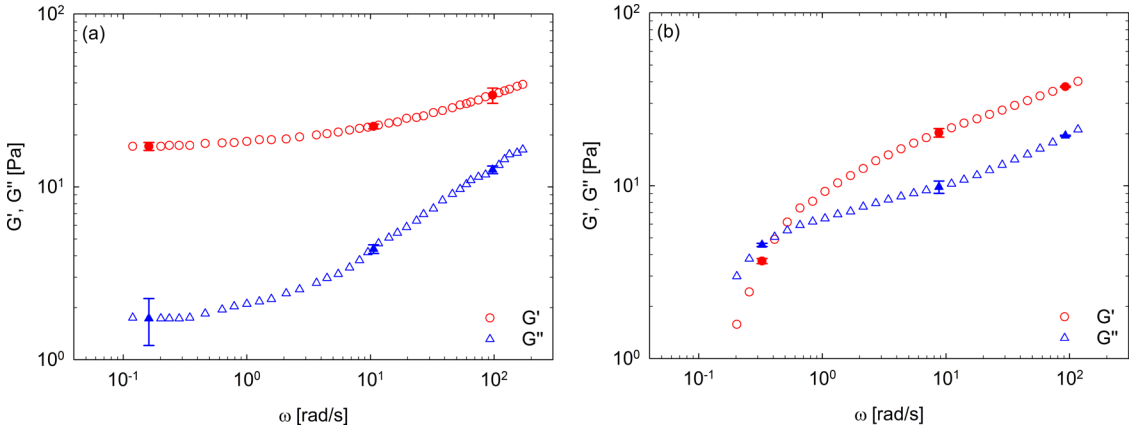


**Figure 5.** Linear viscoelastic behaviors of the Carbopol sample: (a) before yielding (0.1% strain); (b) after yielding (stress of 1 Pa). The error bars are evaluated as the standard deviation of multiple experiments.

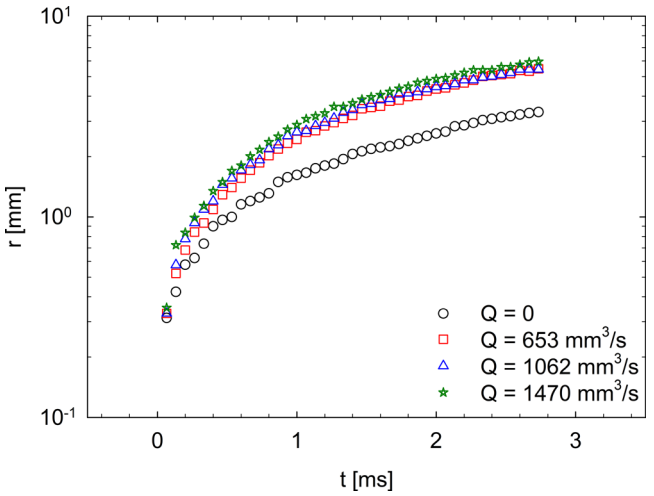


**Figure 6.** Experimental trends of the hole radius $r(t)$ at different $Q$ values for the Carbopol solution.

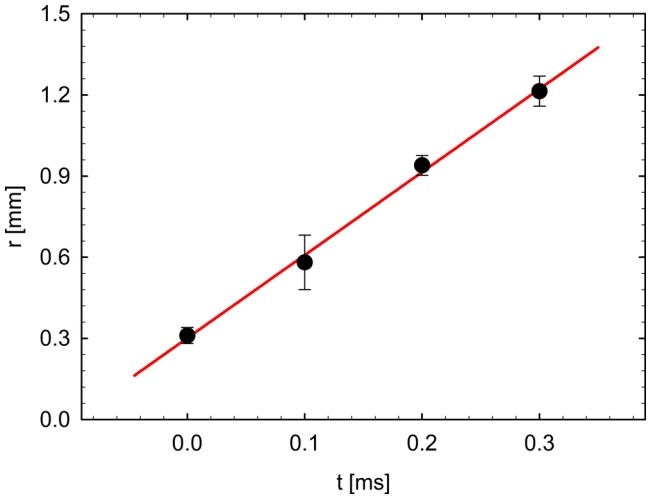


**Figure 7.** Experimental trend of the hole radius $r(t)$ at $Q$ = 1470 mm$^3$/s (data from Figure 6 in the early stages). The slope of the red line gives the value of the initial retracting velocity. The error bars are evaluated as the standard deviation of multiple experiments on the same flow rate.

**Table 1. Experimental Values of the Initial Retracting Velocity for the Carbopol Solution at Different Inflation Rates**

| inflation rate, $Q$ [mm$^3$/s] | experimental initial retracting velocity, $v_0$ [mm/s] |
|---|---|
| 0 | $1.7 \times 10^3 \pm 1.1 \times 10^2$ |
| 653 | $2.5 \times 10^3 \pm 3.6 \times 10^2$ |
| 1062 | $2.6 \times 10^3 \pm 5.7 \times 10^2$ |
| 1470 | $3.1 \times 10^3 \pm 1.7 \times 10$ |

**Table 2. Properties of the Carbopol Solution, at Different Inflation Rates**

| inflation rate, $Q$ [mm$^3$/s] | characteristic velocity, $v_0$ [mm/s] | characteristic shear rate, $\dot{\gamma}$ [s$^{-1}$] | viscosity, $\eta$ [Pa·s] | deformation, $\varepsilon_E$ [dimensionless] |
|---|---|---|---|---|
| 0 | $1.7 \times 10^3$ | $3.4 \times 10^4$ | $3.8 \times 10^{-3}$ | 0 |
| 653 | $2.5 \times 10^3$ | $4.8 \times 10^4$ | $3.1 \times 10^{-3}$ | 0.11 |
| 1062 | $2.6 \times 10^3$ | $5.0 \times 10^4$ | $3.0 \times 10^{-3}$ | 0.17 |
| 1470 | $3.1 \times 10^3$ | $5.9 \times 10^4$ | $2.7 \times 10^{-3}$ | 0.37 |

**Table 3. Dimensionless Numbers for the Carbopol Solution, at Different Inflation Rates**[a]

| inflation rate, $Q$ [mm$^3$/s] | $Re$ | $Ca$ | $Wi$ | $Oh^{-2}$ | $El$ | $E_c$ |
|---|---|---|---|---|---|---|
| 0 | 24 | 0.10 | | 232 | | |
| 653 | 42 | 0.12 | $1.2 \times 10^5$ | 348 | $2.8 \times 10^3$ | $9.9 \times 10^5$ |
| 1062 | 45 | 0.12 | $1.3 \times 10^5$ | 364 | $2.7 \times 10^3$ | $1.0 \times 10^6$ |
| 1470 | 59 | 0.13 | $1.5 \times 10^5$ | 444 | $2.5 \times 10^3$ | $1.1 \times 10^6$ |

[a]For $Q$ = 0, $Wi$, El, $E_c$ cannot be evaluated because of the ideally infinite relaxation time of the unyielded sample.

The fluid density, $\rho$, was always assumed to be equal to that of water. The characteristic length, $\delta$, is the thickness of the fluid film, and it was found to be roughly equal to 0.052 ± 0.017 mm (variance coming from multiple measurements). The surface tension can be estimated to be ~0.063 N/m.[53] The characteristic velocity present in the dimensionless groups was taken as the measured initial retracting velocity of the film, $v_0$, at different values of the inflation rate. The viscosity, $\eta$, is extrapolated using the flow curve at a shear rate value equal to the characteristic shear rate of the process, $\dot{\gamma} = v_0/\delta$. The magnitudes of the computed dimensionless numbers presented in Table 3 suggest that there is an interplay of forces that must


https://doi.org/10.1021/acs.langmuir.2c01875
Langmuir XXXX, XXX, XXX−XXX

be considered, for all the inflation rates. As a result, the whole force balance (eq 6) can be made explicit as follows:

$$v_0^2 + \left(\frac{2\eta}{\rho R_0}\right)v_0 - \frac{2}{\rho}\left(\frac{R_b G'\varepsilon_E}{R_0} + \frac{\gamma}{\delta}\right) = 0 \quad (7)$$

The positive root of eq 7 gives an expression for the initial retracting velocity as follows:

$$v_0 = \frac{1}{2}\sqrt{\left(\frac{2\eta}{\rho R_0}\right)^2 + \frac{8}{\rho}\left(\frac{R_b G'\varepsilon_E}{R_0} + \frac{\gamma}{\delta}\right)} - \frac{\eta}{\rho R_0} \quad (8)$$

Equation 8 represents the retracting velocity where all forces of eq 6 are considered. It can be used to compute the initial retracting velocity for the Carbopol solution at different $Q$ values. While the viscosity enters the model in the viscous retraction term, requiring the use of the value corresponding to the estimated retraction velocity gradient, the choice of the elastic modulus value is based on different grounds. In fact, the elastic modulus was taken at the frequency that corresponds to the $\tan\varphi = G''/G'$ minimum ($\varphi$ is the phase angle), i.e., $\tan\varphi_{min}$ (see the moduli in Figure 5b), equal to 23 Pa for all inflation rates. Such a choice is supported by two considerations. On the one hand, it is known that for entangled polymer systems, the value of $G'$ at $\tan\varphi_{min}$ is a good estimate of the plateau modulus of the material.[54] On the other hand, the elastic term in eq 8 comes from the "loading of the spring", corresponding to the elastic component of the polymer during the inflation stages, preceding the bubble opening. Consequently, the elasticity must correspond to the conditions applied during inflation, where the stress felt by the sample is about 1 Pa (see above), and not during the opening process.

As mentioned above, a metallic cylinder with a radius of 9 mm was used for the experiments. Therefore, the initial radius of the bubble, $R_b$, can be considered equal to about 9 mm. Furthermore, the initial radius of the hole, $R_0$, is equal to 62 $\mu$m, that is, the radius of the tip of the needle. It is worth noting that, if the inflation rate is 0 (null deformation), $F_E = 0$.

Using the parameter values defined above, the numerical derivations of the initial retracting velocity were found using eq 8 and are displayed in Table 4.

**Table 4. Numerical Values of the Initial Retracting Velocity for the Carbopol Solution, at Different Inflation Rates**

| inflation rate, $Q$ [mm$^3$/s] | numerical initial retracting velocity, $v_0$ [mm/s] |
|---|---|
| 0 | $1.5 \times 10^3$ |
| 653 | $1.7 \times 10^3$ |
| 1062 | $1.9 \times 10^3$ |
| 1470 | $2.2 \times 10^3$ |

The retracting velocity for the Carbopol solution is, of course, not dependent on the yield stress, being the puncture performed on a yielded sample characterized by the rheological response in Figure 5b. Furthermore, the ratio that describes the comparison between the yield stress and the capillary pressure is much smaller than 1 ($\sigma_y\delta/\gamma \ll 1$).

The results shown in Table 4 agree well with the experimental outcomes presented in Table 1. The newly derived eq 8 provides a mathematical description of the initial retracting velocity for a viscoelastic fluid, where, in addition to surface tension, inertia is not negligible. It represents an effective means of calculating the initial retracting velocity of a fluid film when the magnitudes of the acting forces are comparable with each other. The initial retracting velocity values found from the experiments and those derived from the mathematical model are compared in Figure 8, as a function of the inflation rate. Although the comparison is not perfect, the model, with no fitted parameters involved, reasonably well predicts the trend of the initial retracting velocity with the flow rate.

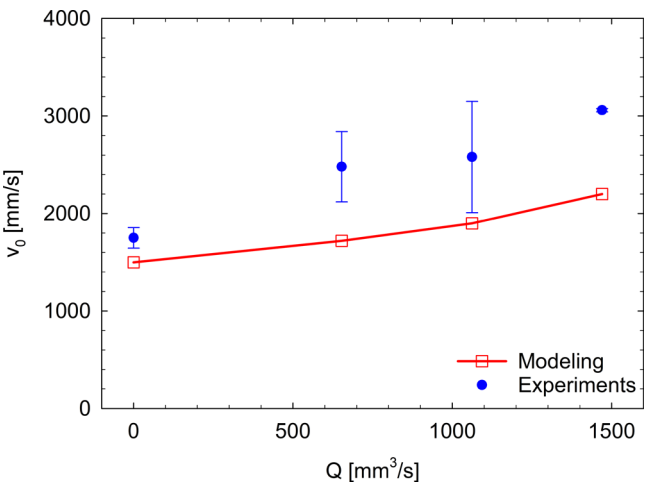


**Figure 8.** Initial retracting velocity as a function of the inflation rate. The error bars are evaluated as the standard deviation of multiple experiments with the same flow rate.

**Comparison with Existing Models.** The comparison between eq 8 and the existing models of the retracting velocity is particularly useful, with the aim of testing the sensitivity of our mathematical model. In Figure 9, we report the trend of $v_0(Q)$ of our model compared to the models of Taylor and Culick,[14,15] Debrégeas et al.,[18,19] and Tammaro et al.[30] Moreover, these predictions are compared with the values of the initial retracting velocities found from the current experiments. It is undeniable that our velocity prediction is the closest to the experimental data, if compared to the other existing models.

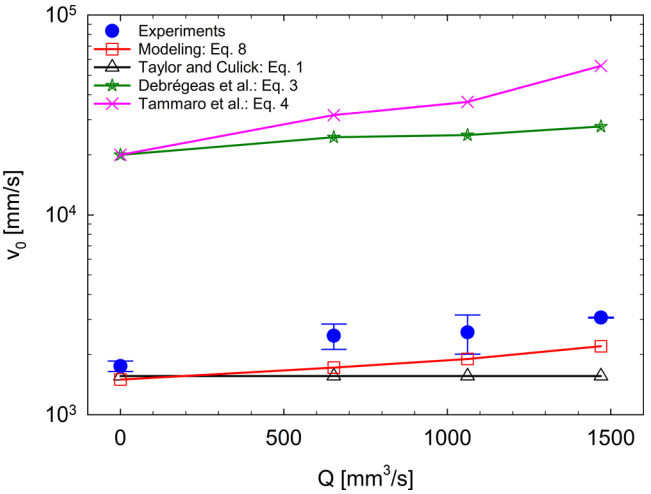


**Figure 9.** Comparison of our experimental and modeling results with predictions from existing models.


https://doi.org/10.1021/acs.langmuir.2c01875
Langmuir XXXX, XXX, XXX−XXX

Table 5. Values of $v_0(Q)$ from Experiments and through eqs 1, 3, 4, and 8

| Q [mm$^3$/s] | experiments, $v_0$ [mm/s] | modeling, $v_0$ [mm/s] | Taylor and Culick, $v_0$ [mm/s] | Debrégeas et al., $v_0$ [mm/s] | Tammaro et al., $v_0$ [mm/s] |
|---|---|---|---|---|---|
| 0 | $1.7 \times 10^3 \pm 1.1 \times 10^2$ | $1.5 \times 10^3$ | $1.6 \times 10^3$ | $2.0 \times 10^4$ | $2.0 \times 10^4$ |
| 653 | $2.5 \times 10^3 \pm 3.6 \times 10^2$ | $1.7 \times 10^3$ | $1.6 \times 10^3$ | $2.4 \times 10^4$ | $3.2 \times 10^4$ |
| 1062 | $2.6 \times 10^3 \pm 5.7 \times 10^2$ | $1.9 \times 10^3$ | $1.6 \times 10^3$ | $2.5 \times 10^4$ | $3.7 \times 10^4$ |
| 1470 | $3.1 \times 10^3 \pm 1.7 \times 10^2$ | $2.2 \times 10^3$ | $1.6 \times 10^3$ | $2.8 \times 10^4$ | $5.6 \times 10^4$ |

The results of this comparison are reported in Table 5.

As previously said, eq 1 of Taylor and Culick comes from a force balance on inviscid liquid films, where the elastic and viscous forces are neglected. Equation 3 of Debrégeas et al. refers to viscous fluids and takes into account the surface tension and viscous contributions, neglecting $F_E$ and $F_I$. Instead, the Tammaro et al. equation (eq 4) for viscoelastic liquids is the result of neglecting only the inertial force. Clearly, the contribution of all terms in eq 8 is essential to achieve the outcomes of Figure 9 and Table 5. In fact, $v_0$ computed using eqs 1, 3, and 4 are markedly different from our $v_0$.

## CONCLUSIONS

Understanding bubble rupture dynamics has an overwhelming importance in many scientific and technological areas. In this paper, we analyzed complex bubble bursting and film retraction phenomena, thanks to a homemade setup and a fast camera.

The experimental investigation involved a non-Newtonian fluid characterized by a peculiar rheology. The rupture dynamics was studied experimentally, by inflating the fluid with different flow rates, and the results were modeled using a dimensionless approach. We derived a novel predictive equation for the computation of the initial retracting velocity, accounting for the elastic force, the viscous force, the inertial force, and the surface tension, and we found good agreement between the experimental outcomes and the mathematical derivations. To test the sensitivity of our mathematical model, we compared it with the existing models of the retracting velocity, which differ from the current one because they do not contemplate one or more of the forces at play. These models predict a velocity that is an order of magnitude higher than the measured one in some cases. The strength of these findings lies in the possibility of characterizing the bubble rupture dynamics of a specific fluid when all the acting forces must be contemplated.

## ASSOCIATED CONTENT

### Supporting Information

The Supporting Information is available free of charge at https://pubs.acs.org/doi/10.1021/acs.langmuir.2c01875.

Figure S1: comparison of three measurements of $r(t)$ at $Q$ = 1062 mm$^3$/s for the 0.10 wt % Carbopol solution (PDF)

## AUTHOR INFORMATION


### Corresponding Author

**Rossana Pasquino** − *DICMaPI, Università degli Studi di Napoli Federico II, 80125 Napoli, Italy;* orcid.org/0000-0003-3513-2794; Email: r.pasquino@unina.it

### Authors

**Nicola Antonio Di Spirito** − *DICMaPI, Università degli Studi di Napoli Federico II, 80125 Napoli, Italy*

**Shadi Mirzaagha** − *DICMaPI, Università degli Studi di Napoli Federico II, 80125 Napoli, Italy*

**Ernesto Di Maio** − *DICMaPI, Università degli Studi di Napoli Federico II, 80125 Napoli, Italy;* orcid.org/0000-0002-3276-174X

**Nino Grizzuti** − *DICMaPI, Università degli Studi di Napoli Federico II, 80125 Napoli, Italy;* orcid.org/0000-0001-5866-609X

Complete contact information is available at: https://pubs.acs.org/10.1021/acs.langmuir.2c01875


### Notes

The authors declare no competing financial interest.

## REFERENCES


(1) de Gennes, P. G.; Brochard-Wyart, F.; Quere, D. *Capillarity and Wetting Phenomena*; Springer, 2003.

(2) Veron, F. Ocean spray. *Annu. Rev. Fluid Mech.* **2015**, *47*, 507−538.

(3) Kientzler, C. F.; Arons, A. B.; Blanchard, D. C.; Woodcock, A. H. Photographic investigation of the projection of droplets by bubbles bursting at a water surface. *Tellus* **1954**, *6*, 1−7.

(4) Spiel, D. E. The sizes of the jet drops produced by air bubbles bursting on sea − and fresh − water surfaces. *Tellus B* **1994**, *46*, 325−338.

(5) Lhuissier, H.; Villermaux, E. Bursting bubble aerosols. *J. Fluid Mech.* **2012**, *696*, 5−44.

(6) Rust, A. C.; Manga, M. Effects of bubble deformation on the viscosity of dilute suspensions. *J. Non-Newtonian Fluid Mech.* **2002**, *104*, 53−63.

(7) Llewellin, E. W.; Manga, M. Bubble suspension rheology and implications for conduit flow. *J. Volcanol. Geotherm. Res.* **2005**, *143*, 205−217.

(8) Mader, H. M.; Llewellin, E. W.; Mueller, S. P. The rheology of two-phase magmas: a review and analysis. *J. Volcanol. Geotherm. Res.* **2013**, *257*, 135−158.

(9) Jones, T. J.; Llewellin, E. W.; Mader, H. M. The use of a shear-thinning polymer as a bubbly magma analogue for scaled laboratory experiments. *J. Volcanol. Geotherm. Res.* **2020**, *392*, No. 106768.

(10) Murray, B. S. Recent developments in food foams. *Curr. Opin. Colloid Interface Sci.* **2020**, *50*, No. 101394.

(11) Duprè, M. A. Sixième memoire sur la theorie mécanique de la chaleur. *Ann. Chim. Phys.* **1867**, *11*, 194−220.

(12) Rayleigh, L. Some applications of photography. *Nature* **1891**, *44*, 249−254.

(13) Ranz, W. E. Some experiments on the dynamics of liquid films. *J. Appl. Phys.* **1959**, *30*, 1950−1955.

(14) Taylor, G. The dynamics of thin sheets of fluid. III. Disintegration of fluid sheets. *Proc. R. Soc. Lond., Ser. A* **1959**, *253*, 313−321.

(15) Culick, F. E. C. Comments on a ruptured soap film. *J. Appl. Phys.* **1960**, *31*, 1128−1129.

(16) McEntee, W. R.; Mysels, K. J. The bursting of soap films. I. An Experimental Study. *J. Phys. Chem. A* **1969**, *73*, 3018−3028.

(17) Keller, J. B. Breaking of liquid films and threads. *Phys. Fluids* **1983**, *26*, 3451−3453.

(18) Debrégeas, G.; Martin, P.; Brochard-Wyart, F. Viscous bursting of suspended films. *Phys. Rev. Lett.* **1995**, *75*, 3886−3891.

(19) Debrégeas, G.; de Gennes, P. G.; Brochard-Wyart, F. The life and death of bare viscous bubbles. *Science* **1998**, *279*, 1704−1707.
(20) Evers, L. J.; Shulepov, S. Yu.; Frens, G. Bursting dynamics of thin free liquid films from Newtonian and viscoelastic solutions. *Phys. Rev. Lett.* **1997**, *79*, 4850−4853.
(21) Brenner, M. P.; Gueyffier, D. On the bursting of viscous films. *Phys. Fluids* **1999**, *11*, 737−739.
(22) Song, M.; Tryggvason, G. The formation of thick borders on an initially stationary fluid sheet. *Phys. Fluids* **1999**, *11*, 2487−2493.
(23) Sünderhauf, G.; Raszillier, H.; Durst, F. The retraction of the edge of a planar liquid sheet. *Phys. Fluids* **2002**, *14*, 198−208.
(24) Dalnoki-Veress, K.; Nickel, B. G.; Roth, C.; Dutcher, J. R. Hole formation and growth in freely standing polystyrene films. *Phys. Rev. E* **1999**, *59*, 2153−2156.
(25) Duchemin, L.; Popinet, S.; Josserand, C.; Zaleski, S. Jet formation in bubbles bursting at a free surface. *Phys. Fluids* **2002**, *14*, 3000−3008.
(26) Savva, N.; Bush, J. W. M. Viscous sheet retraction. *J. Fluid Mech.* **2009**, *626*, 211−240.
(27) Villone, M. M.; D'Avino, G.; Di Maio, E.; Hulsenb, M. A.; Maffettone, P. L. Modeling and simulation of viscoelastic film retraction. *J. Non-Newtonian Fluid Mech.* **2017**, *249*, 26−35.
(28) Villone, M. M.; Hulsen, M. A.; Maffettone, P. L. Numerical simulations of viscoelastic film stretching and relaxation. *J. Non-Newtonian Fluid Mech.* **2019**, *266*, 118−126.
(29) Sabadini, E.; Ungarato, R. F. S.; Miranda, P. B. The elasticity of soap bubbles containing worm like micelles. *Langmuir* **2014**, *30*, 727−732.
(30) Tammaro, D.; Pasquino, R.; Villone, M. M.; D'Avino, G.; Ferraro, V.; Di Maio, E.; Langella, A.; Grizzuti, N.; Maffettone, P. L. Elasticity in Bubble Rupture. *Langmuir* **2018**, *34*, 5646−5654.
(31) Walls, P. L. L.; Henaux, L.; Bird, J. C. Jet drops from bursting bubbles: how gravity and viscosity couple to inhibit droplet production. *Phys. Rev. E* **2015**, *92*, No. 021002.
(32) Ghabache, E.; Séon, T. Size of the top jet drop produced by bubble bursting. *Phys. Rev. Fluids* **2016**, *1*, No. 051901.
(33) Ganan-Calvo, A. M. Revision of Bubble Bursting: Universal Scaling Laws of Top Jet Drop Size and Speed. *Phys. Rev. Lett.* **2017**, *119*, No. 204502.
(34) Lai, C. Y.; Eggers, J.; Deike, L. Bubble Bursting: Universal Cavity and Jet Profiles. *Phys. Rev. Lett.* **2018**, *121*, No. 144501.
(35) Brasz, C. F.; Bartlett, C. T.; Walls, P. L. L.; Flynn, E. G.; Yu, Y. E.; Bird, J. C. Minimum size of the top jet drop from a bursting bubble. *Phys. Rev. Fluids* **2018**, *3*, No. 074001.
(36) Deike, L.; Ghabache, E.; Liger-Belair, G.; Das, A. K.; Zaleski, S.; Popinet, S.; Séon, T. Dynamics of jet produced by a bursting bubble. *Phys. Rev. Fluids* **2018**, *3*, No. 013603.
(37) Botta, O. D.; Magos, I.; Balan, C. Experimental study on the formation and break-up of fluid bubbles. *INCAS Bull.* **2020**, *12*, 27−34.
(38) Sen, U.; Datt, C.; Segers, T.; Wijshoff, H.; Snoeijer, J. H.; Versluis, M.; Lohse, D. The retraction of jetted slender viscoelastic liquid filaments. *J. Fluid Mech.* **2021**, *929*, A25.
(39) Gañán-Calvo, A. M.; López-Herrera, J. M. On the physics of transient ejection from bubble bursting. *J. Fluid Mech.* **2021**, *929*, A12.
(40) Tammaro, D.; Suja, V. C.; Kannan, A.; Gala, L. D.; Di Maio, E.; Fuller, G. G.; Maffettone, P. L. Flowering in bursting bubbles with viscoelastic interfaces. *Proc. Natl. Acad. Sci. U.S.A.* **2021**, *118*, No. e2105058118.
(41) Sanjay, V.; Lohse, D.; Jalaal, M. Bursting bubble in a viscoplastic medium. *J. Fluid Mech.* **2021**, *922*, A2.
(42) Dasouqi, A. A.; Ghossein, J.; Murphy, D. W. The effect of liquid properties on the release of gas from bursting bubbles. *Exp. Fluids* **2022**, *63*, 39−52.
(43) Bridgman, P. W. *Dimensional Analysis*; Yale University Press, 1963.
(44) McKinley, G. H. Dimensionless groups for understanding free surface flows of complex fluids. *SOR Bull.* **2005**, *74*, 6−9.
(45) Denn, M. M.; Porteous, K. C. Elastic effects in flow of viscoelastic liquids. *Chem. Eng. J.* **1971**, *2*, 280−286.
(46) Ohnesorge, W. Die Bildung von Tropfen an Düsen und die Auflösung flüssiger Strahlen. *Z. Angew. Math. Mech.* **1936**, *16*, 355−358.
(47) Anna, S. L.; McKinley, G. H. Elasto-capillary thinning and breakup of model elastic liquids. *J. Rheol.* **2001**, *45*, 115−138.
(48) Benmouffok-Benbelkacem, G.; Caton, F.; Baravian, C.; Skali-Lami, S. Non-linear viscoelasticity and temporal behavior of typical yield stress fluids: carbopol, xanthan and ketchup. *Rheol. Acta* **2010**, *49*, 305−314.
(49) Gutowski, I. A.; Lee, D.; de Bruyn, J. R.; Frisken, B. J. Scaling and mesostructure of Carbopol dispersions. *Rheol. Acta* **2012**, *51*, 441−450.
(50) Graziano, R.; Preziosi, V.; Uva, D.; Tomaiuolo, G.; Mohebbi, B.; Claussen, J.; Guido, S. The microstructure of Carbopol in water under static and flow conditions and its effect on the yield stress. *J. Colloid Interface Sci.* **2021**, *582*, 1067−1074.
(51) Mirzaagha, S.; Pasquino, R.; Iuliano, E.; D'Avino, G.; Zonfrilli, F.; Guida, V.; Grizzuti, N. The rising motion of spheres in structured fluids with yield stress. *Phys. Fluids* **2017**, *29*, No. 093101.
(52) Thompson, R. L.; Sica, L. U. R.; de Souza Mendes, P. R. The yield stress tensor. *J. Non-Newtonian Fluid Mech.* **2018**, *261*, 211−219.
(53) Jørgensen, L.; Le Merrer, M.; Delanoe-Ayari, H.; Barentin, C. Yield stress and elasticity influence on surface tension measurements. *Soft Matter* **2015**, *11*, 5111−5121.
(54) Larson, R. G.; Sridhar, T.; Leal, L. G.; McKinley, G. H.; Likhtman, A. E.; McLeish, T. C. B. Definitions of entanglement spacing and time constants in the tube model. *J. Rheol.* **2003**, *47*, 809−818.




https://doi.org/10.1021/acs.langmuir.2c01875
*Langmuir* XXXX, XXX, XXX−XXX